Synthesis of kaliophilite by alkaline fusion and ultrasonic treatment method from kaolin raw material

Cynthia Aristeo-Domínguez [1], Marissa Vargas-Ramírez [1], Ana M. Herrera-González [1], Jesús García-Serrano [1], Alejandro Téllez-Jurado [2], Alejandro Cruz-Ramírez [3]

[1] Instituto de Ciencias Básicas e Ingeniería, Universidad Autónoma del Estado de Hidalgo (UAEH), México

[2] Laboratorio de Agrobiotecnología, Universidad Politécnica de Pachuca, Zempoala, Hidalgo, México

[3] Departamento de Formación Profesional Genérica. Instituto Politécnico Nacional – Unidad Profesional Interdisciplinaria de Ingeniería campus Hidalgo (UPIIH-IPN), México

Corresponding author: alcruzr@ipn.mx (Alejandro Cruz-Ramírez)

Abstract: Mexico has important kaolin deposits, which must be assessed to obtain products with a high commercial value, such as kaliophilite as raw material for biodiesel production. Two kaolins, A and B, with approximate $SiO_2:Al_2O_3$ ratios of 1 and 1.2, respectively, were used as raw materials to produce kaliophilite. Both kaolins were obtained from the municipality of Agua Blanca in the State of Hidalgo, Mexico. Kaolins are a source of Al and Si for the synthesis of kaliophilite through an alkali fusion process at 700 °C followed by ultrasonic treatment at 28 kHz to different times and for Kaolin-KOH ratios of 1:1 and 1:1.2 (mass: mass). The kaolins as received and the alkaline mixtures heat and ultrasonically treated were analyzed using X-ray diffraction (XRD), Fourier-transform infrared spectroscopy (FT-IR), thermogravimetric analysis (TGA), and scanning electron microscopy with energy-dispersive X-ray spectroscopy (SEM-EDS). The most suitable kaolin for synthesizing kaliophilite was kaolin A with the Si/Al mass ratio of approximately 1, which exhibited a higher crystallinity index range from 54 to 79.6%. Higher KOH concentrations promote the amorphous material formation decreasing the kaliophilite amount. The crystallinity index was increased when the time of ultrasonic treatment was increased.

Keywords: kaolin, alkaline fusion, ultrasonic treatment, kaliophilite

1. Introduction

Feldspathoids, a group of aluminosilicates with a unique composition featuring lower silica content than feldspars, have diverse applications. They are extensively employed in ethylbenzene dehydrogenation to styrene, steam reforming of hydrocarbons for hydrogen production, ammonia synthesis for industrial and construction applications, and as a promising heterogeneous catalyst for biodiesel (Ellis et al., 2015; Esaifan et al., 2016; He et al., 2019; Okamoto & Kawahara, 1996; Wen et al., 2010). Kaliophilite ($KAlSiO_4$) is a feldspathoid with a zeolite-like structure comprising interconnected tetrahedra $(SiO_4)^{4-}$ and $(AlO_4)^{5-}$ (Okamoto & Kawahara, 1996). In 1958, Tuttle and Smith successfully obtained synthetic kaliophilite, referred to as kaliophilite H_2 by Merlino in 1984. Okamoto, in 1997, refined its structure, noting its hexagonal symmetry (P63mc) with a = 5.17 and c = 8.49 Å. Kaliophilite has been synthesized by several researchers mainly using hydrothermal and fusion methods. The hydrothermal method has been successfully employed to produce kaliophilite from fly ash raw material such as the works of He et al. (2019) and Chen et al. (2022). He et al. (2019) synthesized kaliophilite catalysts for biodiesel production using the hydrothermal method, mixing ash with KOH at 80°C and subsequently treating the sample in an autoclave at 180°C for 24 hours. The kaliophilite synthesized showed a high crystallinity and purity. Later, Chen et al. (2022) examined the effect of alkali concentration in the synthesis of kaliophilite from fly ash with high calcium content using the hydrothermal method. Mixtures of ash with different concentrations of KOH were cured at 8°C for 24 hours, followed by treatment in an autoclave at 180°C for 48 hours. It was determined that high alkali

concentrations contributed to the formation of kaliophilite. The fusion method has been applied mainly for the synthesis of kaliophilite from kaolin raw material in a carbonated medium. Heller-Kallai and Lapides (2003) synthesized kaliophilite from $KAlSiO_4$ minerals using thermal treatments. Mixtures of kaolinite and potassium carbonate in a 1:10 solid-to-solid ratio were heat treated at 700°C for 1 hour generating synthetic kaliophilite as the main product and kalsilite as a byproduct. Later, Novembre and Gimeno (2017) studied the effects of time and temperature on the synthesis process of $KAlSiO_4$ polymorphs including kaliophilite. Calcined kaolin at 650° was mixed with K_2CO_3 in a 1:1 solid-to-solid ratio as starting materials. The results showed that kalsilite and $KAlSiO_4$-01 were synthesized at 700°C and 800°C, respectively leading to the formation of synthetic H2 kaliophilite as a metastable phase. Subsequently, Mahloujifar and Mansournia (2018) synthesized kaliophilite, kalsilite, trikalsilite, and nepheline from solid mixtures of kaolin and K_2CO_3 in a molar ratio of 1:1.2 through the fusion method in a range from 800°C to 1100°C wherein kaliophilite was obtained at 800°C and 900°C. Its particular properties such as numerous basic potassium active sites and insolubility in vegetable oil and methanol make kaliophilite a promising heterogeneous catalyst for biodiesel production, among other applications like diesel soot reduction, refractory materials, as a catalyst in biodiesel production, and in agglomerate formation in fluidized bed reactors (Becerro et al., 2009; Cook et al., 1977; He et al., 2019; G. Wang et al., 2018). However, the main area of opportunity lies in the development of catalysts for biodiesel production, given the substantial international trade in biodiesel (13% of global production) (OECD, 2023). On the other hand, ultrasound is used in various industries including mineral processing to enhance separation recoveries and obtain better-quality products at acceptable and bearable costs. Furthermore, in the case of chemical processes including leaching and electrolysis, ultrasound also increases the process efficiencies at lower retention times and chemical dosages by increasing the surface area of the particles and creating more reactive surfaces (Gungoren et al, 2024). The use of high-frequency (> 20 kHz) processing or ultrasonic vibrations is a powerful way to disperse and homogenize different solid particles dispersed in water. It has been shown that the use of ultrasound in the production of feldspars such as zeolites from kaolin can improve the efficiency, quality, and homogeneity of the synthesis process (Park et al., 2001) because ultrasonic waves provide unique reaction conditions through acoustic cavitation and can propagate in different materials to enhance the processes (Bang & Suslick, 2010). Kaolin clay is a dioctahedral phyllosilicate produced through the chemical weathering of aluminum silicate minerals such as feldspar. It is typically white, but iron oxide imparts pink, orange, and red hues, giving it a distinctive tone (Adeoye et al., 2018). It is a layered silicate mineral, with a tetrahedral sheet linked through oxygen atoms to an octahedral sheet of alumina, having the chemical composition $Al_2Si_2O_5(OH)_4$ (Deer, 1997). In Mexico, numerous kaolin deposits are widely distributed, mainly in the Trans-Mexican Volcanic Belt (Hernández Chávez et al., 2021), with significant deposits in the states of Guanajuato, Hidalgo, and Veracruz (De Pablo-Galán 1979). The extraction of kaolin holds considerable economic importance, serving as a cost-effective, abundant, non-corrosive raw material in the synthesis of geopolymers, mesoporous aluminosilicates, and zeolite microporous structures. Its applications span various industries, including ceramics, rubber compounds, inks, plastics, cosmetics, construction materials, paints, paper, absorbents, and catalysis (Ayele et al., 2015; Barrer et al., 1968; Doyle et al., 2016; Ekosse, 2010; Heah et al., 2011; Mahloujifar & Mansournia, 2018; Murray, 1991; Mymrin et al., 2018; Ramírez-Ortiz et al., 2011). The kaolins produced in Mexico are used mainly as a raw material for the ceramic industry. However, the unique characteristics of kaolin make it an attractive raw material for exploring its potential in the production of feldspathoids like kaliophilite. Therefore, this study aims to perform thermal treatments of K-doped kaolins through alkali fusion followed by ultrasonic treatment from Mexican kaolin raw material as starting materials in kaliophilite synthesis.

2. Materials and methods

In this study, two types of kaolin from the municipality of Agua Blanca in the state of Hidalgo were used for the synthesis of kaliophilite as a source of Al and Si. The chemical composition (Table 1) was previously reported (Hernández-Chávez et al., 2021) by using plasma emission spectrophotometry ICP-OES with a Perkin Elmer Optima 8300 model and the procedure reported by P. J. Potts (2003) while the mineralogical quantification was performed by the Rietveld Method using Bruker's TOPAS 4.2 software

and the procedure reported by R. Cheary and A. Coelho (1992) for the kaolin raw material. Potassium hydroxide (KOH) powder with 85% purity was employed for the alkali activation of the kaolins.

Table 1. Characteristics of the kaolin raw materials composition (mass %)

	Kaolin clay A		Kaolin clay B	
	Chemical	Mineralogical	Chemical	Mineralogical
SiO_2	46.65	Kaolinite = 21 (±2)	46.38	Kaolinite = 46 (±3)
Al_2O_3	44.27	Quartz = 7 (±1)	36.86	Quartz = 12 (±2)
Fe_2O_3	0.14	Cristobalite = 26 (±3)	0.81	Cristobalite = 4 (±2)
K_2O	0.1	Tridymite = 39 (±2)	1.34	Tridymite = 24 (±3)
TiO_2	0.09	Alunite = 7 (±1)	0.66	Alunite = 14 (±2)

The procedure was carried out separately for each kaolin, referred to as "kaolin A" (with SiO_2:Al_2O_3 ratio ~ 1) and "kaolin B" (with SiO_2:Al_2O_3 ratio ~ 1.2).

Powdered KOH was mixed with each kaolin at two solid-to-solid ratios, 1:1 and 1:1.2. The samples were placed in crucibles and thermally treated in a muffle furnace at 700°C for 2 hours to eliminate hydroxyl (OH) groups from their rupture and induce a high degree of disorder to form metakaolin, which is highly, reactive (Breck, 1984; P. Wang et al., 2019). After the reaction time, the samples were extracted, cooled through thermal shock to room temperature, and allowed to rest for 24 hours. Subsequently, water was added, and they underwent ultrasonic treatment at 70°C for 2 hours at a frequency of 28 kHz (Table 2). After the reaction time, the products were rinsed with distilled water, filtered, and dried at 60°C. For both kaolins, thermal treatment followed by ultrasound was performed for the 1:1 kaolin-KOH composition at 4, 8, 12, and 16 hours (Table 2). In Table 2, the sample nomenclature is as follows: the ultrasonic treatment time, the kaolin type, and the mass ratio mixture.

Table 2. Experimental composition of the starting mixtures for the alkali fusion treatment at 700°C followed by ultrasonic treatment at a frequency of 28 kHz

Kaolin	Sample	Kaolin:KOH m:m	Time (h)
A	2A2	1:1.2	2
	2A1	1:1	2
	4A1	1:1	4
	8A1	1:1	8
	12A1	1:1	12
	16A1	1:1	16
B	2B2	1:1.2	2
	2B1	1:1	2
	4B1	1:1	4
	8B1	1:1	8
	12B1	1:1	12
	16B1	1:1	16

The raw kaolins and the products resulting from the thermal treatment were characterized by X-ray Spectroscopy, using an INEL X-ray diffractometer, model EQUINOX 2000, with monochromatic Co Kα radiation (λ = 1.78901 Å) operating in θ/2θ configuration, with an angular data acquisition range from 10 to 70°. The corresponding functional groups in the raw kaolins and synthesized products were identified by Infrared Spectroscopy using an Agilent Cary 630 FT-IR spectrometer. The analyzed wavenumber range fluctuated between 4000 and 450 cm^{-1}. Thermal analyses of the raw kaolin samples and synthesized products were conducted using Mettler Toledo TGA Thermogravimetric Analysis. A

heating rate of 10 °C min^{-1} was applied with a nitrogen flow rate of 50 mL min^{-1} in alumina crucibles, within a temperature range from 50 to 1200 °C. To reveal the microstructure and perform a qualitative analysis of the synthesized products, a JEOL JSM-6701F scanning electron microscope with energy-dispersive X-ray spectroscopy (SEM-EDS) analysis was employed. An Au-Pd film was deposited on the powder surfaces to make them conductive. Images were obtained at various magnifications using backscattered electrons.

3.   Results and discussion

3.1. X-ray Diffraction (XRD)

The samples subjected to thermal treatment and before ultrasonic treatment were characterized by X-ray powder diffraction to determine their phase transformations. Figs. 1 and 2 show the XRD patterns of samples from kaolin A and B as received and heat treated to 700°C, besides the products obtained from kaolin-KOH samples after heat treated at 700 °C for 2 hours, and the solid phases obtained after subjecting the kaolin-KOH mixtures to ultrasonic treatment at 28 kHz for two hours. In Fig. 1a, the presence of kaolinite (PDF 01-078-1996), tridymite (PDF 00-016-0152), quartz (PDF 01-089-8938), cristobalite (PDF 01-085-0621), in smaller proportion alunite (PDF 01-071-1776), and anatase (PDF 01-071-1169) is observed. After the calcination of kaolin A for 2 hours at 700 °C (fig. 1b), the XRD pattern confirms the transformation of kaolinite to metakaolinite, as most peaks corresponding to kaolinite disappear (Wang et al., 2019), although three peaks of kaolinite, one of tridymite, two of cristobalite, and two of quartz remain. The thermal treatment of kaolin produces a noticeable change in the composition of the crystalline phase around 700 °C, which can be attributed to the dehydroxylation of structural OH in kaolinite. The disappearance of most peaks belonging to quartz and cristobalite is related to their transformation into amorphous silica because of the thermal treatment. The disappearance of all peaks corresponding to alunite can be explained by the loss of water molecules from the kaolin mineral, leading to its disappearance (Khan et al., 2017; G. Wang et al., 2019). The XRD pattern for kaolin A subjected to 700 °C shows that the complete formation of metakaolinite is not achieved due to the perseverance of the kaolinite, tridymite, cristobalite, and quartz peaks. The XRD pattern for the kaolin A-KOH 1:1 mixture after alkali fusion with KOH at 700 °C shows a structural modification, as it exhibits the appearance of a peak at approximately 33.62° 2θ corresponding to synthetic kaliophilite (PDF 00-012-0134), eliminating the characteristic peaks of the raw kaolin A sample (Fig. 1c). After subjecting the kaolin A-KOH 1:1 to ultrasonic treatment at 28 kHz and 70 °C for 2 hours (sample 2A1) (Fig. 1d), XRD peaks corresponding to synthetic kaliophilite (PDF 00-012-0134) are observed at approximately 24.59°, 26.35°, 34°, 40.55°, 47.60°, and 50.10° 2θ (Smith & Tuttle, 1957). Similarly, the kaolin A-KOH 1:1.2 subjected to 700 °C shows a total modification in its structure due to the appearance of a characteristic peak of potassium aluminum silicate (PDF 00-018-0987) at approximately 37.56° 2θ (Fig. 1e). The XRD pattern for the kaolin A-KOH 1:1.2 composition after being expound to 700 °C followed by ultrasonic irradiation (2A2) (Fig. 1f) presents broadband corresponding to amorphous geopolymer at approximately 27.90° to 42.95° 2θ (Autef et al., 2013; He et al., 2019). The kaolin A-KOH 1:1 favors the formation of kaliophilite besides higher concentration of KOH negatively impacts the formation of kaliophilite; therefore, ultrasonic treatment trials were performed only for the sample 2A1 at the times of 4, 8, 12, and 16 h to 28 kHz frequency and 70 °C.

Fig. 2 shows the XRD patterns obtained for kaolin B for the as-received condition and after heat treatments for raw material and kaolin B-KOH mixtures heat treated and with ultrasonic treatment. The XRD pattern for kaolin B (Fig. 2a) shows a similar behavior related to kaolin A, the presence of kaolinite, tridymite, quartz, cristobalite, alunite, and anatase is observed. In the XRD pattern corresponding to kaolin B after being calcined at 700 °C for 2 hours (Fig. 2b), the disappearance of most peaks belonging to kaolinite is observed, indicating that the material underwent partial transformation to metakaolinite (Wang et al., 2019). A similar behavior regarding kaolin A is observed, impurities of quartz, tridymite, and cristobalite persist, and all peaks corresponding to alunite and anatase disappear, but retain an anatase peak, indicating a partial formation of metakaolinite. It is observed that the kaolin B-KOH 1:1 mixture after alkali fusion at 700 °C (Fig. 2c) shows structural modification, with the appearance of peaks at approximately 33.28°, 36.30°, 37.56°, and 39.50° 2θ corresponding to potassium aluminum silicate, along with a peak corresponding to synthetic kaliophilite at approximately34° 2θ. Similar to
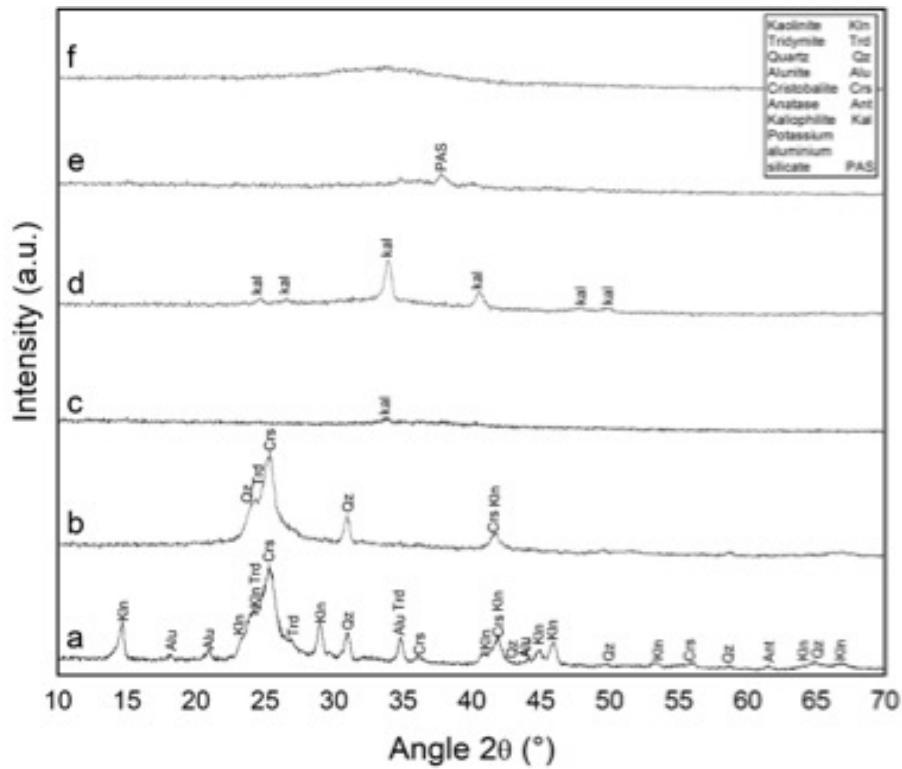
Fig. 1. XRD patterns of the samples a) raw kaolin A, b) kaolin A thermally treated at 700 °C, c) kaolin A-KOH mixture in proportions 1:1 subjected to 700 °C, d) kaolin A-KOH mixture in proportions 1:1 after ultrasonic treatment, e) kaolin A-KOH mixture in proportions 1:1.2 subjected to 700 °C, and f) kaolin A-KOH mixture in proportions 1:1.2 after ultrasonic treatment
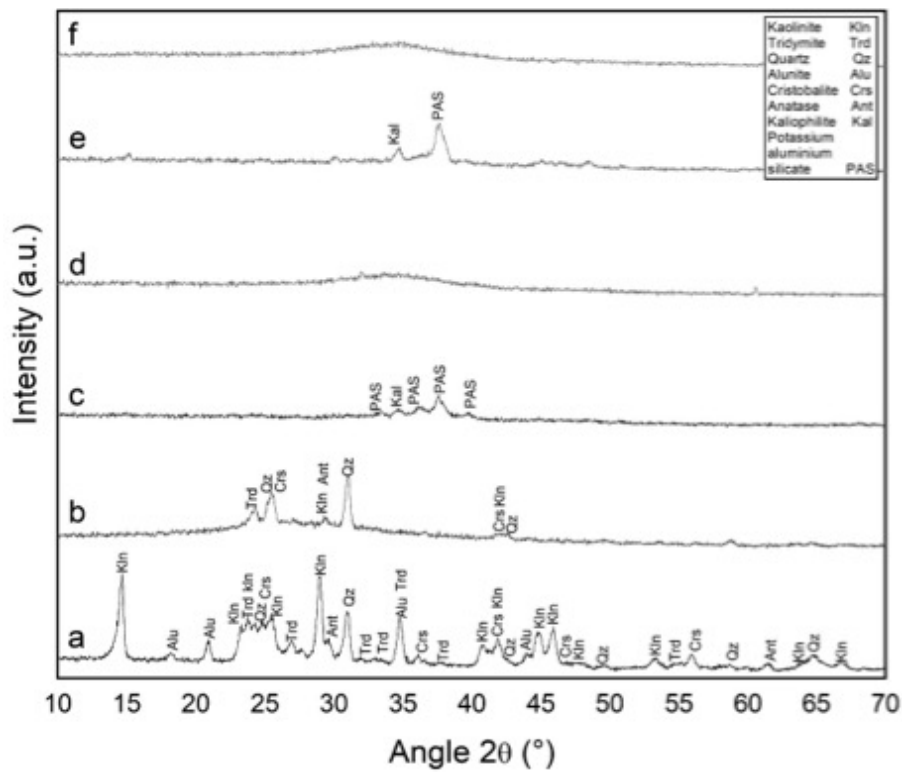

Fig. 2. XRD patterns of the samples a) raw kaolin B, b) kaolin B thermally treated at 700 °C, c) kaolin B-KOH mixture in proportions 1:1 subjected to 700 °C, d) kaolin B-KOH mixture in proportions 1:1 after ultrasonic treatment, e) kaolin B-KOH mixture in proportions 1:1.2 subjected to 700 °C, and f) kaolin B-KOH mixture in proportions 1:1.2 after ultrasonic treatment

kaolin A, there is a total disappearance of characteristic peaks of the raw kaolin B sample. After undergoing kaolin B to alkali fusion and 2 hours of ultrasonic treatment at 28 kHz and 70 °C, it is observed that the kaolin B-KOH 1:1 (sample 2B1) (Fig. 2d) presents a broadband corresponding to amorphous geopolymer between 24.50° and 42.50° 2θ (Autef et al., 2013; He et al., 2019). The kaolin B-KOH 1:1 subjected to alkali fusion at 700 °C shows a characteristic peak of kaliophilite at 34° and a peak of potassium aluminum silicate at 37.56° 2θ (Fig. 2e), indicating a total modification in its structure while the sample 2B2 (Fig. 2f) presents a broadband corresponding toamorphous geopolymer between 24.50° and 42.50° 2θ (Autef et al., 2013; He et al., 2019). The behavior of Kaolin B-KOH 1:1.2 after the thermal and ultrasonic treatments show that a higher content of alkali promotes the formation of an amorphous geopolymer while kaolinite is obtained for the lowest KOH addition, thus the effect of the ultrasonic treatment (28kHz and 70°C) to different times (4, 8, 12, and 16 h) was evaluated only for the sample 2B1 previously heat treated.

The XRD patterns of the kaolin A-KOH 1:1 mixture after being subjected to 28 kHz ultrasonic treatment for 2, 4, 8, 12, and 16h are shown in Fig. 3. Peaks corresponding to hexagonal kaliophilite (Chen et al., 2022; Mahloujifar & Mansournia, 2018; Smith & Tuttle, 1957; J. Wang et al., 2023) are present at approximately 24.74°, 26.35°, 34°, 40.55°, 48.01°, and 50.1° 2θ (Figs. 3b to 3f). At reaction times of 4, 8, 12, and 16h, an additional peak appears at 23.40° 2θ, also attributed to kaliophilite. Additionally, it is observed that the XRD peaks of kaliophilite exhibit higher intensities in the peaks of samples 4A1, 8A1, 12A1, and 16A1 than in sample 2A1 with the shortest ultrasonic treatment while the sample treated at the longest time (sample 16A1) shows the most intense peaks. The positive effect on the intensity of kaliophilite peaks is due to the fact that the use of high-frequency processing or ultrasonic vibrations is a powerful way to disperse and homogenize different solid particles dispersed in water (Furtado et al., 2004; Sauter et al.,2008).

Fig. 4 shows the XRD patterns of the samples of the kaolin B-KOH 1:1 after ultrasonic treatment at 28 kHz for 2, 4, 8, 12, and 16h. The XRD patterns for samples 4B1, 8B1, 12B1 and 16B1, show an amorphous band between 24.50° to 42.50° of 2θ, from which two peaks stand out at 34° and 40.54° of 2θ corresponding to kaliophilite (Figs. 4c to 4f). According to the raw material composition (Table 1), kaolin B exhibits higher percentages of impurities such as Fe_2O_3, K_2O, and TiO_2 (0.81%, 1.34%, and 0.66%
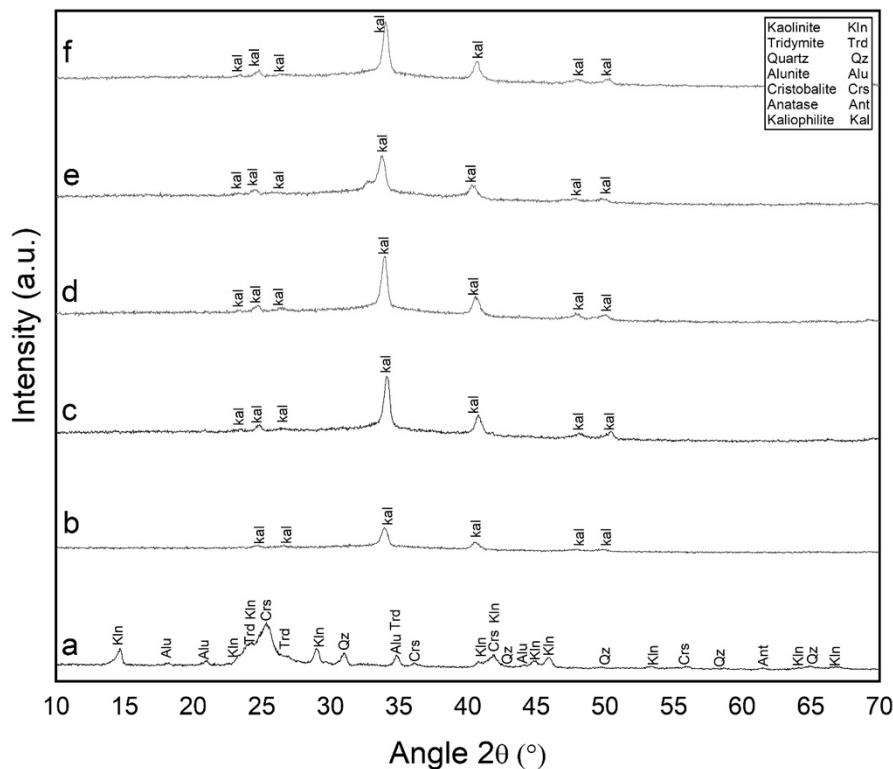

Fig. 3. XRD patterns of the sample a) raw kaolin A and kaolin A-KOH 1:1 mixtures after alkali fusion and ultrasonic treatment at 28 kHz for b) 2h, c) 4h, d) 8h, e) 12h, and f) 16h

respectively) compared to kaolin A (0.14% Fe_2O_3, 0.1% K_2O, and 0.09% TiO_2). These impurities play a crucial role in the synthesis of kaliophilite, where iron, in particular, affects the physicochemical properties of kaolin, hurting the quality of the final product (Ramaswamy & Raghavan, 2011). In this context, it was found that kaolin A, with a lower content of impurities, was more suitable for the synthesis of kaliophilite. In contrast, the impurities present in kaolin B hindered the formation of kaliophilite, as reflected in the presence of an amorphous band in sample 2B1 and the presence of two kaliophilite peaks in the X-ray diffraction patterns of samples 4B1, 8B1, 12 B1, and 16B1 (Fig. 4).
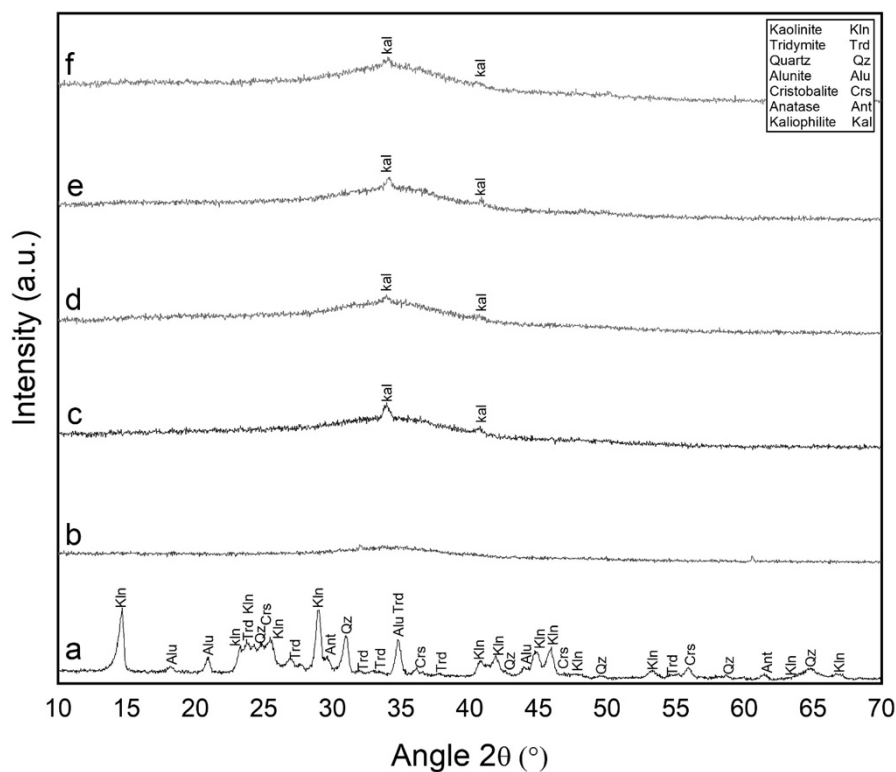

Fig 4. XRD patterns of sample a) raw kaolin B and kaolin B-KOH 1:1 mixtures after fusion and ultrasonic treatment at 28 kHz for b) 2h, c) 4h, d) 8h, e) 12h, and f) 16h

From the X-ray diffraction patterns, the integration of the area under the crystalline peaks and the total area of the X-ray pattern was conducted using the ORIGINPRO 2023b software. Subsequently, the crystallinity index was assessed following the equation 1 (Hato et al., 2017; Navarro-Pardo et al., 2013).

$$CI(\%) = \frac{AC}{AT} x100 \tag{1}$$

where AC is area of the crystalline domain and AT is total area of the domain.

Table 3 shows the crystallinity index for both kaolin-KOH samples determined from the results obtained in Figs. 3 and 4. It is observed that the kaolin B samples exhibit a lower crystallinity index ranging from zero to 13.98%. On the other hand, in the kaolin A samples, a crystallinity index is presented in the range of 54.14 to 79.61%. The kaliophilite synthesized for the longest ultrasonic treatment shows the highest crystallinity index.

Table 3. Crystallinity Index

Sample	Crystallinity Index (%)	Sample	Crystallinity Index (%)
2A1	54.14	2B1	0
4A1	65.46	4B1	13.98
8A1	71.79	8B1	8.83
12A1	63.98	12B1	11.69
16A1	79.61	16B1	7.96

3.2. Fourier Transform Infrared Spectroscopy (FT-IR)

Figs. 5 and 6 show the FT-IR spectra corresponding to raw kaolin A and kaolin B, respectively, and their corresponding mixtures with KOH after alkaline fusion and ultrasonic treatment. The spectrum corresponding to kaolin A registers characteristic bands for kaolinite (fig. 5a). The bands at 3693, 3650, and 3621 cm^{-1} correspond to external OH groups bonded to aluminum (Ayeni et al., 2021; Erasmus, 2016; Ilic et al., 2010; Koutnik, 2019; Sruthi & Reddy P, 2017). The band at 3485 cm^{-1} corresponds to the O-H stretching of the water contained in the kaolin (Ayeni et al., 2021; Mahloujifar & Mansournia, 2018). The band at 1020 cm^{-1} corresponds to Si-O stretching bonds (Ilic et al., 2010), and the band at 912 cm^{-1} corresponds to the Al-OH bond in the internal structure (Erasmus, 2016; Ilic et al., 2010; Mahloujifar & Mansournia, 2018; Souri et al., 2015). The flexion of the Al-O and Si-O bonds is found between the bands at 789 and 681 cm^{-1} (Koutnik, 2019). The band at 540 cm^{-1} represents Al-O-Si bonds (Ilic et al., 2010; Khan et al., 2017; Souri et al., 2015), the band at 460 cm^{-1} corresponds to the T-O-T bending bond (T: Si or Al) (Koutnik, 2019), and the band at 424 cm^{-1} corresponds to the Si-O vibrational bond (Koutnik, 2019). Fourier Transform Infrared Spectroscopy (FT-IR) was employed to identify the change of phases in the Kaolin A-KOH samples after ultrasonic treatment at different times (Figs. 5b to 5f). The results match with those obtained in the XRD patterns, i.e., the characteristic bands of kaolinite between 3693 and 3621 cm^{-1} disappear (Esaifan et al., 2016). The broad bands at 3413 and 1640 cm^{-1} indicate absorbed water (Mahloujifar & Mansournia, 2018), while the band at 1120 cm^{-1} represents the transformation from the amorphous phase to kaliophilite (Mahloujifar & Mansournia, 2018). Additionally, the main bands of kaliophilite appear at 973, 690, and 607 cm^{-1} (Chen et al., 2022), showing a significant shift in the vibrations of the antisymmetric stretching Si-O-T (T: Si or Al) bonds, which in kaolinite are located at 1020 cm^{-1} and shift to 973 cm^{-1} upon the formation of kaliophilite (Esaifan et al., 2016). The bands at 690 and 607 cm^{-1} indicate the formation of characteristic six-membered rings of kaliophilite (Chen et al., 2022), corresponding to symmetric stretching vibrations of the Si (Al)-O bond (He et al., 2019). The bands at 557 and 478 cm^{-1} are attributed to the bending vibrations of the Si-O bond (He et al., 2019), and the band at 427 cm^{-1} indicates internal vibrations of Si-O-Aloct (Mahloujifar & Mansournia, 2018). It can be observed that the intensity of the bands is lower at the 2-hour mark (Fig. 5b) and increases from 4h onwards (Figs. 5c to 5f), which is attributed to the longer residence time in the ultrasonic treatment bath.
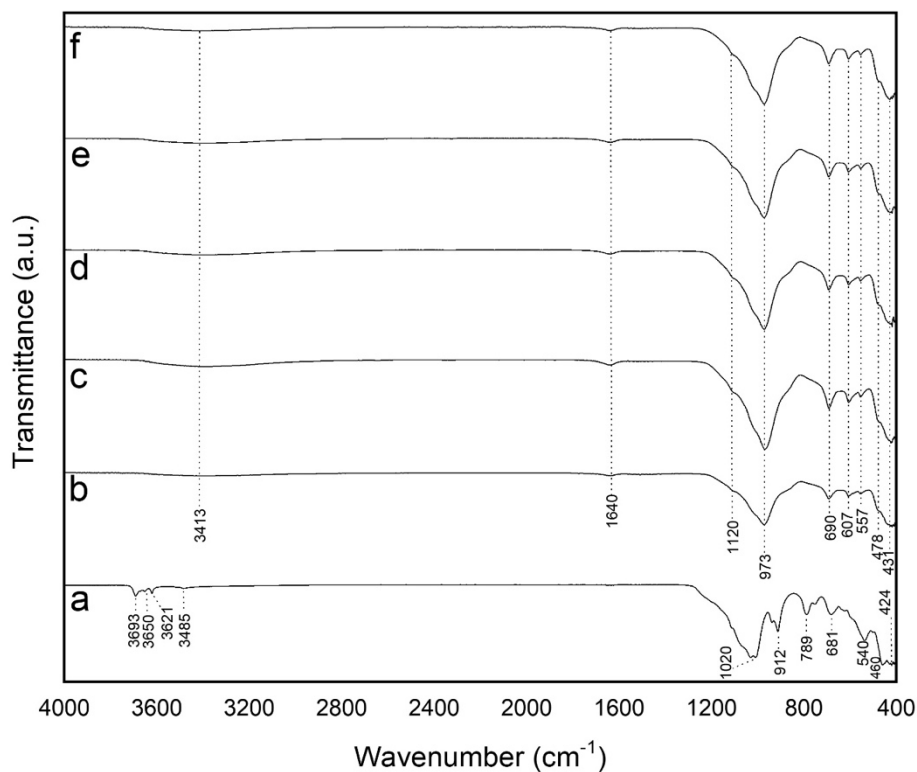

Fig. 5. FT-IR spectra of the sample a) raw kaolin A and the kaolin A-KOH 1:1 mixtures after alkali fusion and ultrasonic treatment at 28 kHz for b) 2h, c) 4h, d) 8h, e) 12h, and f) 16h

From Fig. 6, it is observed that the characteristic bands of kaolinite between 3691 and 3621 cm^{-1} disappear (Esaifan et al., 2016), and the intensity of the bands for the kaolinite obtained from kaolin B is lower than the bands for the kaolinite obtained in kaolin A. It is observed that the complete transformation from the amorphous phase to kaliophilite was not achieved, as the formation of the band around 1120 cm^{-1} is not observed, as was the case in the spectra of kaliophilite from kaolin A. The presence of a single band indicating the formation of characteristic six-membered rings of kaliophilite at 685 cm^{-1} is evident, while the band at 607 cm^{-1} is absent. The band at 478 cm^{-1}, attributed to Si-O bending vibrations, is also not present in the FT-IR spectra for the kaolin B-KOH mixtures (Figs. 6b to 6f). The FT-IR results are consistent with the findings in the XRD patterns, and in general, are similar to the FT-IR spectra results of kaolin A.
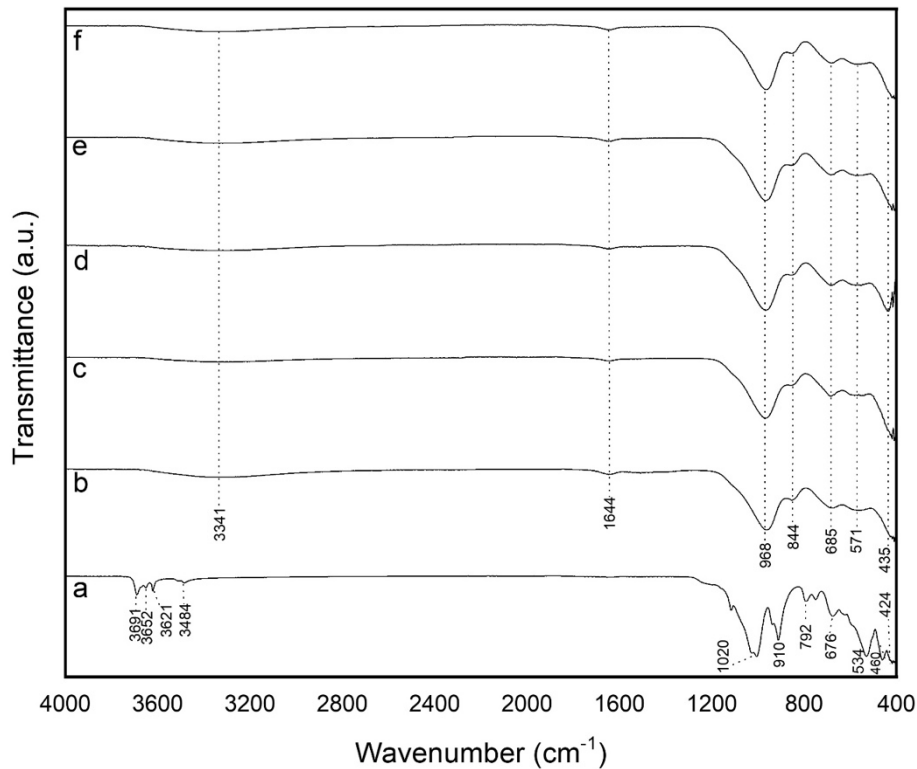

Fig. 6. FT-IR spectra of sample a) raw kaolin B and the kaolin B-KOH 1:1 mixtures after alkali fusion and ultrasonic treatment at 28 kHz during b) 2h, c) 4h, d) 8h, e) 12h, and f) 16h

3.3. Thermogravimetric Analysis (TGA)

Figs. 7 and 8 display the TGA thermograms of samples from raw kaolins A and B, as well as samples treated thermally with KOH and ultrasonic treatment. The TGA curve for raw kaolin A shows a weight reduction of approximately 15.58% (fig. 7), while the TGA curve for raw kaolin B exhibits a weight loss of approximately 17.9% (fig. 8). The initial weight loss is attributed to water loss and the burning of organic materials at low temperatures. kaolin minerals undergo dehydroxylation in the range of 500 to 600 °C, and the decomposition of kaolin occurs in the range of 700 to 800 °C, where alunite ($KAl(SO_4)_2$) decomposes into K_2SO_4, Al_2O_3, and SO_3 around 710 °C (Hernández Chávez et al., 2021). The kaolin A-KOH 1:1 mixtures and kaolin B-KOH 1:1 mixture shown in Figs. 7 and 8, respectively experienced mass reductions with increasing temperature. For samples subjected to alkali fusion followed by ultrasonic treatment of the kaolin A-KOH 1:1 mixture, a weight reduction ranging from approximately 24.89% to 16.08% was recorded, with sample 2A1 exhibiting the highest weight reduction (~24.89%) and sample 16A1 showing the lowest weight loss (~16.08%). Similarly, the kaolin B-KOH 1:1 mixture showed a weight loss ranging from around 32.90% to 17.90%, with sample 2B1 exhibiting the highest weight loss (~32.90%) and sample 4B1 showing the lowest weight loss (~18.15%). This weight loss trend was exclusively due to the loss of water through the evaporation of free water and condensation of hydroxyl groups (Duxson et al., 2006), correlating with their crystallinity percentage (Table 3). For both kaolins,

the samples with the shortest ultrasonic treatment (2A1 and 2B1) presented the highest weight loss due to their lower crystallinity percentage, allowing more space for water molecules to move easily and be eliminated. In the range from 50 to 200 °C, absorbed surface water was lost from the materials (Prud'homme et al., 2011; Selmani et al., 2017). After 200 °C, dehydroxylation occurred due to the alkaline component (KOH) added to the mixtures (Prud'homme et al., 2011).
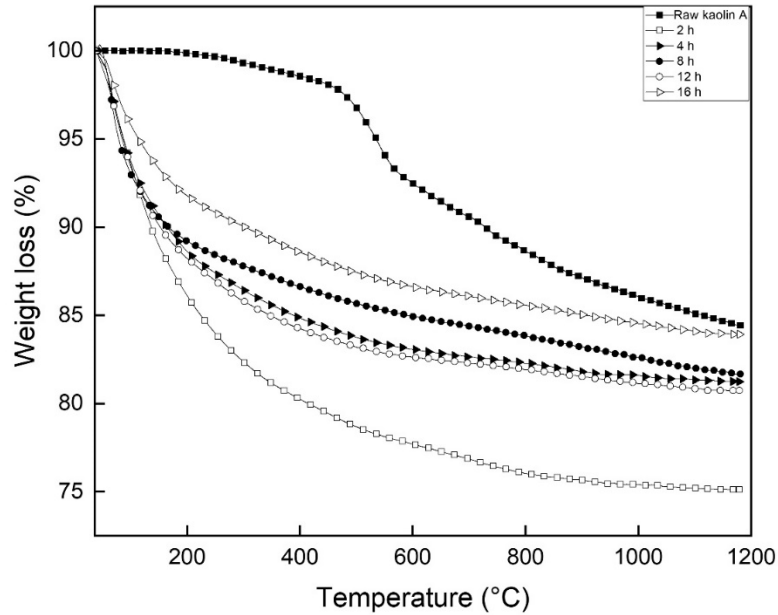

Fig. 7. TGA curves of raw kaolin A samples and kaolin A-KOH 1:1 mixture after being subjected to alkali fusion followed by ultrasonic treatment at 28 kHz for 2, 4, 8, 12, and 16 hours
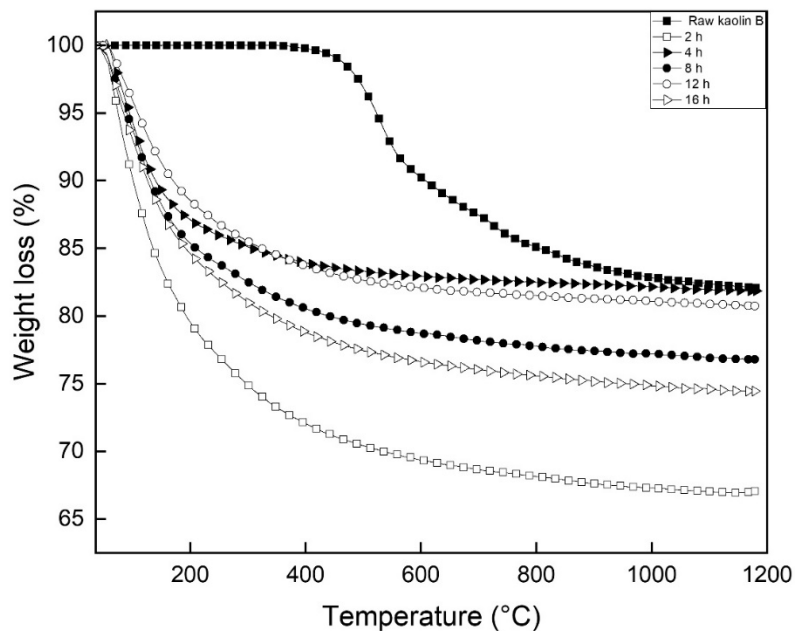

Fig. 8. TGA curves of raw kaolin B samples and kaolin B-KOH 1:1 mixture after being subjected to alkali fusion followed by ultrasonic treatment at 28 kHz for 2, 4, 8, 12, and 16 hours

3.4. Scanning Electron Microscope (SEM)

Fig. 9 shows the SEM-EDS images of raw kaolin A samples and kaolin A-KOH 1:1 mixture after ultrasonic treatment for 2, 4, 8, 12, and 16 hours. In Fig. 9a, hexagonal flakes consisting of coarse and compact grains display the characteristic morphology of kaolinite (Lee et al., 2003). Morphological

changes in kaolin A clay after treatment with KOH are confirmed through SEM micrographs, revealing the formation of kaliophilite crystals (Mahloujifar & Mansournia, 2018; Sruthi et al., 2020; Sruthi & Reddy P, 2017; Yao et al., 2011) which fit with XRD results. The micrograph for the two-hour ultrasonic treatment (Fig. 9b) shows the formation of agglomerated kaliophilite structures. Additionally, as the ultrasonic treatment time increases, nanoscale particles of kaliophilite are produced showing greater residual porosity (Figs. 9c, 9d, 9e, and 9f). EDS results for kaolin A (Fig. 9a) indicate the presence of Al, Si, and O, corresponding mainly to kaolinite and silica polymorphs, aligning with XRD results. Moreover, EDS analysis of the samples with the ultrasonic treatment confirms the presence of kaliophilite composed of O, Si, Al, and K.
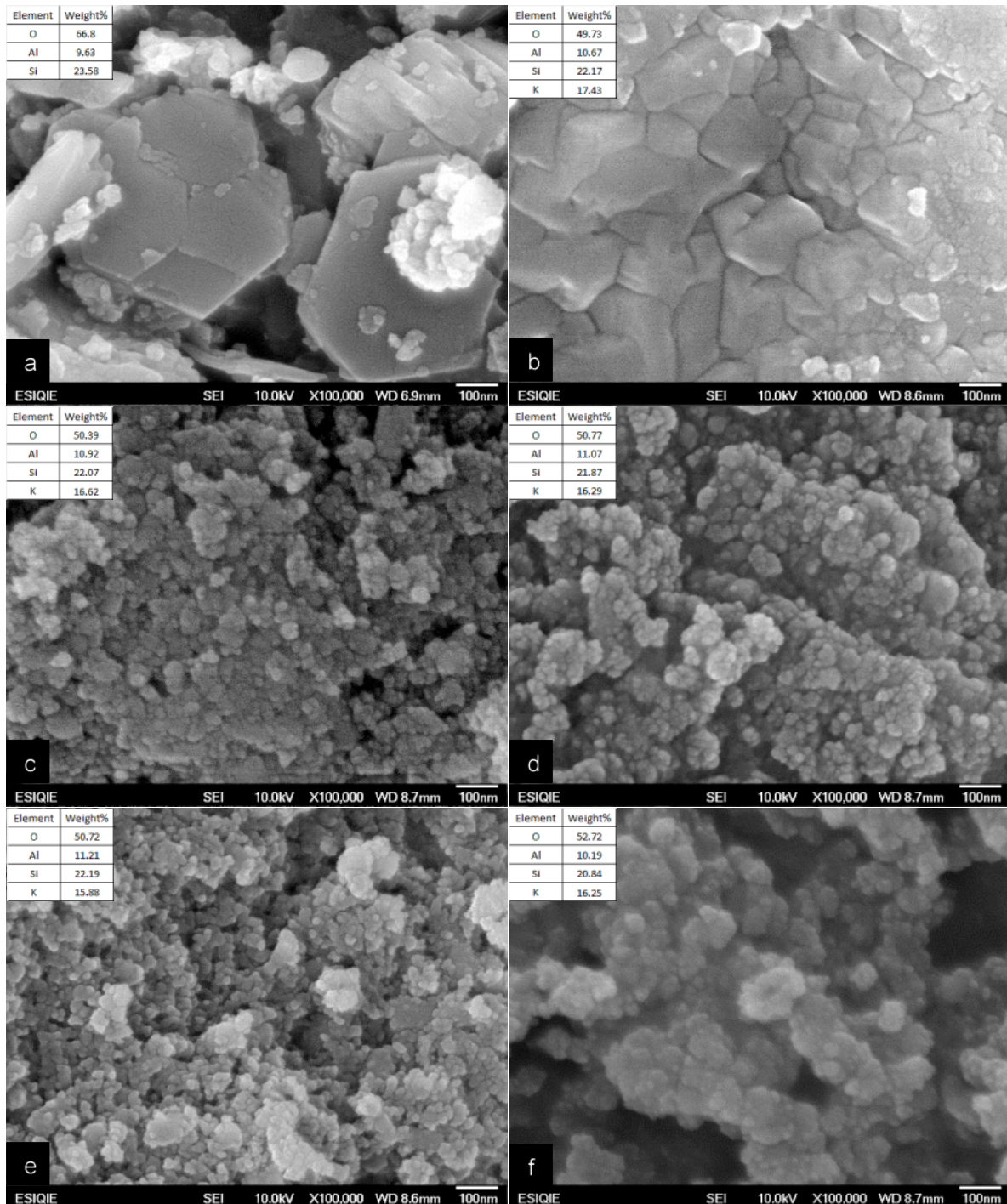
Fig. 9. SEM micrographs of a) raw kaolin A and kaolin A-KOH 1:1 mixture after alkaline fusion and ultrasonic treatment at 28 kHz during b) 2h, c) 4h, d) 8h, e) 12h, and f) 16h. The EDS results are displayed in the SEM micrographs

In Fig. 10, SEM-EDS images of raw kaolin B and kaolin B-KOH 1:1 samples are presented. Raw kaolin B (Fig. 10a) shows similar morphologies to kaolin A, this is hexagonal flakes with the characteristic morphology of kaolinite. After ultrasonic treatment for 2, 4, 8, 12, and 16 hours, the formation of kaliophilite is observed, appearing as nanostructures more clustered and less regular than the structures obtained for kaolin A-KOH 1:1 mixture. Microanalysis of kaolin B shows high amounts of Al, Si, and O within the structures of kaolinite and silica polymorphs. Additionally, impurities of K, Ti, and S are present, corresponding to the minerals alunite and anatase observed in the XRD pattern. EDS results for 1:1 kaolin B-KOH mixtures confirm the presence of kaliophilite composed of O, Si, Al, and K, and fit with the XRD results.

The experimental route followed in this work that involves an alkaline fusion at 700 °C followed by
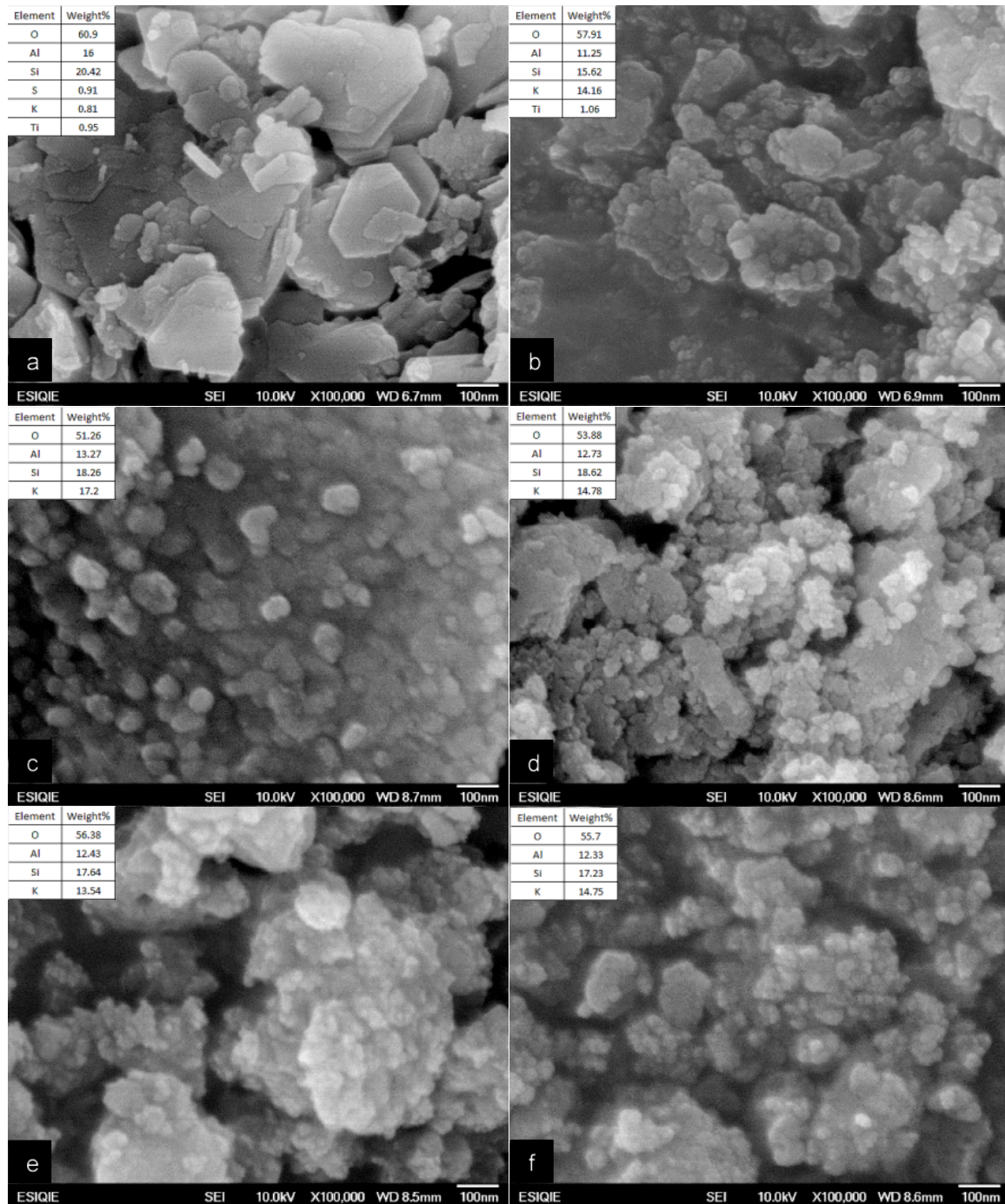

Fig. 10. SEM micrographs of a) raw kaolin B and the 1:1 kaolin B-KOH mixtures after alkaline fusion and ultrasonic treatment at 28 kHz for b) 2h, c) 4h, d) 8h, e) 12h, and f) 16h. EDS results are displayed in the SEM micrographs

ultrasonic treatment at 70 °C allowed the synthesis of kaliophilite at a lower temperature than those used by Mahloujifar and Mansournia in 2018 (800 °C and 900 °C) and He et al. in 2019 (1000 °C). The proposed experimental route represents a lower energy consumption. Furthermore, the kaliophilite produced as the sole product was stable without becoming unstable over time, unlike in previous studies where kaliophilite H2 became unstable (Heller-Kallai and Lapides, 2003) (Novembre and Gimeno, 2017). This ability to produce kaliophilite as the sole reaction product at a lower temperature while ensuring its stability represents a significant advancement in mineral synthesis from kaolin raw material.

Kaolin deposits are widely distributed in Mexico, usually located in the Trans-Mexican Volcanic Belt. Agua Blanca in Hidalgo and Huayacocotla in Veracruz are two economically important, well-known kaolin deposits (De Pablo-Galán, 1978). Based on the mineralogical and thermal properties of the kaolins evaluated, they are suitable as a raw material for the ceramic industry. However, the results obtained in this research establish an experimental methodology that allows the formation of kaliophilite mainly in kaolin A-KOH mixtures obtained by a combined heat treatment process with ultrasonic treatment. This processing route represents a potential alternative to expand the processing options for Mexican industrial kaolins. The obtained kaliophilite has potential application in the development of kaliophilite catalysts, making it suitable for evaluation in the biodiesel production industry. This could contribute to the development of more efficient and sustainable processes, aligning with the growing demand for biofuels and the need for environmentally friendly production methods. Therefore, kaliophilite synthesis holds promise for advancing the biodiesel industry and supporting the transition to renewable energy sources.

4. Conclusions

In this work, the synthesis of kaliophilite from kaolin raw material was carried out successfully through alkali fusion with KOH additions, followed by ultrasonic treatment. The conclusions obtained are as follows:

1. Raw kaolin samples consist of kaolinite, alunite, tridymite, cristobalite, quartz, and anatase. The Si/Al mass ratio of approximately 1 in kaolin A allowed for obtaining kaliophilite with adequate crystallinity for the ultrasonic treatment for 16 h.
2. The kaolins heat treated to 700 °C followed by ultrasonic treatment at 28 kHz for 2 hours allow to obtain synthetic kaliophilite as the main product in the kaolin A-KOH 1:1 (mass: mass) mixture and an amorphous geopolymer in the kaolin B-KOH 1:1 mixture. The Si/Al mass ratio of approximately 1.2 in kaolin-KOH mixtures promotes amorphous material formation. Thus, higher KOH concentrations can negatively impact kaliophilite formation.
3. The kaolins heat treated to 700 °C followed by ultrasonic treatment at 28 kHz for different times allow the formation of kaliophilite for kaolin A-KOH mixtures while kaolin B-KOH mixtures show an amorphous band with a small amount of kaliophilite. The higher crystallinity index (79.61%) was obtained for kaolin A-KOH mixtures for the longest ultrasonic treatment.
4. Phase changes identified by DRX were confirmed by FTIR, with the disappearance of characteristic kaolinite bands and the appearance of bands corresponding to kaliophilite in both kaolin mixtures after the thermal and ultrasonic treatments while SEM-EDS showed kaliophilite crystals in both mixtures; however, the kaolin A-KOH 1:1 presented regular morphologies and less agglomerated structures than kaolin B-KOH 1:1 mixtures.

Acknowledgments

References

ADEOYE, J.B., OMOLEYE, J.A., OMOLEYE, M.E., 2018. *Development of alum from kaolin deposit using response surface methodology.* MOJ Bioorganic & Organic Chemistry. 2(3), 166-169.

AUTEF, A., PRUD'HOMME, E., JOUSSEIN, E., GASGNIER, G., PRONIER, S., ROSSIGNOL, S., 2013. *Evidence of a gel in geopolymer compounds from pure metakaolin*. Journal of Sol-Gel Science and Technology. 67(3), 534-544.

AYELE, L., PÉREZ-PARIENTE, J., CHEBUDE, Y., & DÍAZ, I., 2015. *Synthesis of zeolite A from Ethiopian kaolin*. Microporous and Mesoporous Materials. 215, 29-36.

AYENI, O., ONWUALU, A. P., BOAKYE, E., 2021. *Characterization and mechanical performance of metakaolin-based geopolymer for sustainable building applications*. Construction and Building Materials. 272, 121938.

BANG, J.H., SUSLICK, K. S., 2010. *Applications of Ultrasound to the Synthesis of Nanostructured Materials*. Advanced Materials. 22(10), 1039-1059.

BARRER, R.M., COLE, J.F., STICHER, H., 1968. *Chemistry of soil minerals. Part V. Low-temperature hydrothermal transformations of kaolinite*. Journal of the Chemical Society A: Inorganic, Physical, Theoretical. 0, 2475-2485.

BECERRO, A. I., ESCUDERO, A., MANTOVANI, M., 2009. *The hydrothermal conversion of kaolinite to kalsilite: Influence of time, temperature, and pH.* American Mineralogist. 94(11-12), 1672-1678.

BRECK, D. W., 1984, *Zeolite Molecular Sieves: Structure, Chemistry, and Use.* R.E. Krieger.

CHEN, X., CHEN, J., LI, M., WANG, J., ZHOU, Z., DU, P., ZHANG, X., 2022. *Synthesis of kaliophilite from high calcium fly ash: Effect of alkali concentration*. Case Studies in Construction Materials. 17, e01542.

COOK, L.P., ROTH, R. S., PARKER, H. S., NEGAS, T., 1977. *The system $K_2O-Al_2O_3-SiO_2$; Part 1, Phases on the $KAlSiO_4$-$KAlO_2$ join.* American Mineralogist. 62(11-12), 1180-1190.

CHEARY, R.W., COELHO, A.A., 1992. *A fundamental parameters approach to X-ray line-profile fitting*, J. Appl. Cryst. 25(2), 109-121.

DE PABLO-GALAN, L., 1979. *The Clay Deposits of Mexico*. In M. M. Mortland & V. C. Farmer (Eds.), Developments in Sedimentology (Vol. 27, pp. 475-486). Elsevier.

DEER, W.A., 1997. *Rock forming minerals / W.A. Deer, R.A. Howie, J. Zussman. Vol. 1A, Orthosilicates.* (Second edition / Repr. with corrections.). Geological Society.

DOYLE, A.M., ALBAYATI, T.M., ABBAS, A.S., ALISMAEEL, Z.T., 2016. *Biodiesel production by esterification of oleic acid over zeolite Y prepared from kaolin*. Renewable Energy. 97, 19-23.

DUXSON, P., LUKEY, G.C., VAN DEVENTER, J.S.J., 2006. *Thermal evolution of metakaolin geopolymers: Part 1 – Physical evolution*. Journal of Non-Crystalline Solids. 352(52-54), 5541-5555.

EKOSSE, G.-I.E., 2010. *Kaolin deposits and occurrences in Africa: Geology, mineralogy and utilization.* Applied Clay Science. 50(2), 212-236.

ELLIS, N., MASNADI, M.S., ROBERTS, D.G., KOCHANEK, M.A., ILYUSHECHKIN, A.Y., 2015. *Mineral matter interactions during co-pyrolysis of coal and biomass and their impact on intrinsic char co-gasification reactivity*. Chemical Engineering Journal. 279, 402-408.

ERASMUS, E., 2016. *The influence of thermal treatment on properties of kaolin*. Hemijska industrija. 70(5), 595-601.

ESAIFAN, M., KHOURY, H., ALDABSHEH, I., RAHIER, H., HOURANI, M., WASTIELS, J., 2016. *Hydrated lime/potassium carbonate as an alkaline activating mixture to produce kaolinitic clay-based inorganic polymer.* Applied Clay Science. 126, 278-286.

FURTADO, C.A., KIM, U.J., GUTIERREZ, H.R., PAN, L., DICKEY, E.C., EKLUND, P.C., 2004. *Debundling and Dissolution of Single-Walled Carbon Nanotubes in Amide Solvents*. J. Am. Chem. Soc. 126 (19), 6095–6105.

GUNGOREN, C., OZKAN, S. G., OZDEMIR, O., 2024. *Use of Ultrasound in Physical and Chemical Mineral Processing Operations*. In S. J. Ikhmayies (Ed.), Advances in Minerals Research, 25-54. Springer Nature Switzerland.

HATO, M.J., MOTAUNG, T.E., CHOI, H.J., SCRIBA, M., KHUMALO, V.M., MALWELA, T., 2017. *Effect of organoclay on the properties of maleic-anhydride grafted polypropylene and poly(methyl methacrylate) blend*. Polymer Composites, 38(3), 431-440.

HE, P.Y., ZHANG, Y.J., CHEN, H., HAN, Z. C., LIU, L.C., 2019. *Low-energy synthesis of kaliophilite catalyst from circulating fluidized bed fly ash for biodiesel production*. Fuel. 257, 116041.

HEAH, C.Y., KAMARUDIN, H., BAKRI, A. M. M. A., BINHUSSAIN, M., LUQMAN, M., NIZAR, I. K., RUZAIDI, C.M., LIEW, Y.M., 2011. *Effect of Curing Profile on Kaolin-based Geopolymers*. Physics Procedia. 22, 305-311.

HELLER-KALLAI, L., LAPIDES, I., 2003. *Thermal reactions of kaolinite with potassium carbonate*. Journal of Thermal Analysis and Calorimetry. 71, 689–698.

HERNÁNDEZ CHÁVEZ, M., VARGAS RAMÍREZ, M., HERRERA GONZÁLEZ, A., GARCÍA SERRANO, J., CRUZ RAMÍREZ, A., ROMERO SERRANO, J., SÁNCHEZ ALVARADO, R., 2021. *Thermodynamic analysis of the influence of potassium on the thermal behavior of kaolin raw material*. Physicochemical Problems of Mineral Processing. 57(1), 39-52.

ILIC, B., MITROVIC, A., MILICIC, L., 2010. *Thermal treatment of kaolin clay to obtain metakaolin*. Hemijska Industrija. 64(4), 351-356.

KHAN, M.I., KHAN, H.U., AZIZLI, K., SUFIAN, S., MAN, Z., SIYAL, A.A., MUHAMMAD, N., FAIZ UR REHMAN, M., 2017. *The pyrolysis kinetics of the conversion of Malaysian kaolin to metakaolin*. Applied Clay Science. 146, 152-161.

KOUTNIK, P., 2019. *Comparison of kaolin and kaolinitic claystones as raw materials for preparing meta-kaolinite-based geopolymers*. Ceramics – Silikaty. 110-123.

LEE, S., KIM, Y.J., MOON, H.-S., 2003. *Energy-Filtering Transmission Electron Microscopy (EF-TEM) Study of a Modulated Structure in Metakaolinite, Represented by a 14 Å Modulation*. Journal of the American Ceramic Society. 86(1), 174-176.

MAHLOUJIFAR, M., MANSOURNIA, M., 2018. *Kaolinite fusion in carbonate media: KAlSiO 4 –NaAlSiO 4 phase transformations and morphological study*. Materials Research Express. 6(2), 025040.

MERLINO, S., 1984. *Feldspathoids: Their Average and Real Structures*. On W. L. Brown (Ed.), Feldspars and Feldspathoids (pp. 435-470). Springer Netherlands.

MURRAY, H. H., 1991. *Overview – Clay mineral applications*. Applied Clay Science. 5(5-6), 379-395.

MYMRIN, V., SANTOS, C.F.G., ALEKSEEV, K., AVANCI, M.A., KREUSCH, M.A., BORGA, T., GRAUPMANN, O., CAVALIN, F. L., MONTEIRO, R.A., RUY, V.A., 2018. *Influence of kaolin clay on mechanical properties and the structure formation processes of white ceramics with inclusion of hazardous laundry sewage sludge*. Applied Clay Science. 155, 95-102.

NAVARRO-PARDO, F., MARTÍNEZ-BARRERA, G., MARTÍNEZ-HERNÁNDEZ, A., CASTAÑO, V., RIVERA-ARMENTA, J., MEDELLÍN-RODRÍGUEZ, F., VELASCO-SANTOS, C., 2013. *Effects on the Thermo-Mechanical and Crystallinity Properties of Nylon 6,6 Electrospun Fibres Reinforced with One-Dimensional (1D) and Two-Dimensional (2D) Carbon*. Materials. 6(8), 3494-3513.

NOVEMBRE, D., GIMENO, D., 2017. *The Solid-state Conversion of Kaolin to Kalsio 4 Minerals: The Effects of Time and Temperature*. Clays and Clay Minerals. 65(5), 355-366.

OECD., 2023. *OECD-FAO Agricultural Outlook 2023-2032*. OECD. https://doi.org/10.1787/08801ab7-en

OKAMOTO, Y., 1997. *Structural Modification of KAISi04 Minerals*. Earth Science Reports. 3(1), 57-64.

OKAMOTO, Y., KAWAHARA, A., 1996. *Interpretation of the Crystal Structure of Synthetic Kaliophilite from the Domain Structure of Kalsilite*. Okayama Univ. Earth Science Reports. 3(1), 57-64.

PARK, J., KIM, B.C., PARK, S.S., PARK, H.C., 2001. *Conventional versus ultrasonic synthesis of zeolite 4A from kaolin*. Journal of Materials Science Letters. 20, 531-533.

POTTS, P. J., 2003. Handbook of rock analysis. Science.

PRUD'HOMME, E., MICHAUD, P., JOUSSEIN, E., CLACENS, J.-M., ARII-CLACENS, S., SOBRADOS, I., PEYRATOUT, C., SMITH, A., SANZ, J., ROSSIGNOL, S., 2011. *Structural characterization of geomaterial foams – Thermal behavior*. Journal of Non-Crystalline Solids. 357(21), 3637-3647.

RAMASWAMY, S., RAGHAVAN, P., 2011. *Significance of Impurity Mineral Identification in the Value Addition of Kaolin – A Case Study with Reference to an Acidic Kaolin from India*. Journal of Minerals and Materials Characterization and Engineering, 10(11), 1007-1025.

RAMÍREZ-ORTIZ, J., MEDINA-VALTIERRA, J., ROSALES, M.M., 2011. *Used Frying Oil for Biodiesel Production Over Kaolinite as Catalyst*. World Academy of Science, Engineering and Technology, Open Science Index 56. International Journal of Chemical and Biological Engineering. 5(8), 710-713.

SAUTER, C., EMIN, M. A., SCHUCHMANN, H. P., TAVMAN, S., 2008. *Influence of Hydrostatic Pressure and Sound Amplitude on the Ultrasound Induced Dispersion and De-agglomeration of Nanoparticles*. Ultrason. Sonochem. 15(4), 517–523.

SELMANI, S., SDIRI, A., BOUAZIZ, S., JOUSSEIN, E., ROSSIGNOL, S., 2017. *Effects of metakaolin addition on geopolymer prepared from natural kaolinitic clay*. Applied Clay Science. 146, 457-467.

SMITH, J. V., & TUTTLE, O. F., 1957. *The nepheline-kalsilite system; Part I, X-ray data for the crystalline phases*. American Journal of Science. 255(4), 282-305.

SOURI, A., GOLESTANI-FARD, F., NAGHIZADEH, R., VEISEH, S., 2015. *An investigation on pozzolanic activity of Iranian kaolins obtained by thermal treatment*. Applied Clay Science. 103, 34-39.

SRUTHI, P.L., REDDY P.H.P., 2017. *Characterization of kaolinitic clays subjected to alkali contamination*. Applied Clay Science. 146, 535-547.

SRUTHI, P.L., REDDY, P.H.P., MOGHAL, A.A.B., 2020. *Role of Alkali Concentration on the Micro-Level Characteristics of Kaolinitic Clay*. Geo-Congress. 189-198.

TUTTLE, O.F., SMITH, J.V., 1958. *The nephelinekalsilite system; II, Phase relations*. American Journal of Science, 256(8), 571-589.

WANG, G., JENSEN, P.A., WU, H., FRANDSEN, F.J., LAXMINARAYAN, Y., SANDER, B., GLARBORG, P., 2019. *KOH capture by coal fly ash*. Fuel. 242, 828-836.

Wang, G., Jensen, P. A., Wu, H., Frandsen, F. J., Sander, B., & Glarborg, P., 2018. *Potassium Capture by Kaolin, Part 1: KOH*. Energy & Fuels. 32(2), 1851-1862.

WANG, J., CHEN, X., LI, C., ZHOU, Z., DU, P., ZHANG, X., 2023. *Evaluating the effect of kaliophilite on the fire resistance of geopolymer concrete*. Journal of Building Engineering. 75, 106975.

WANG, P., SUN, Q., ZHANG, Y., CAO, J., 2019. *Synthesis of Zeolite 4A from Kaolin and Its Adsorption Equilibrium of Carbon Dioxide*. Materials. 12(9), 1536.

WEN, G., YAN, Z., SMITH, M., ZHANG, P., WEN, B., 2010. *Kalsilite based heterogeneous catalyst for biodiesel production*. Fuel. 89(8), 2163-2165.

YAO, Z., XIA, M., YE, Y., ZHANG, L., 2011. *Kaliophilite from fly ash: Synthesis, characterization, and stability*. Bulletin of Materials Science. 34(7), 1671-1674.